# Computation of Separated Transonic Turbulent Flows

George S. Deiwert*
*NASA Ames Research Center, Moffett Field, Calif.*

**The two-dimensional Reynolds averaged compressible Navier-Stokes equations are solved using MacCormack's second-order accurate explicit finite difference method to simulate the separated transonic turbulent flowfield over an airfoil. Four different algebraic eddy viscoisity models are tested for viability to achieve turbulence closure for the class of flows considered. These models range from an unmodified boundary-layer mixing-length model to a relaxation model incorporating special considerations for the separation bubble region. Results of this study indicate the necessity for special attention to the separated flow region and suggest limits of applicability of algebraic turbulence models to these separated flowfield.**

## Introduction

WITH the advent of large high-speed computers and accurate and efficient numerical algorithms, recent attention has been given to the computation of separated turbulent compressible flowfields.[1-11] In each of these studies the time-dependent Reynolds averaged Navier-Stokes equations for two-dimensional compressive flow are used and turbulence closure is achieved by means of model equations for the Reynolds stresses. Wilcox[1,2] used a first-order accurate numerical scheme and the two equation differential turbulence model of Saffman[12] to simulate the supersonic shock boundary-layer interaction experiment of Reda and Murphy[13] and the compression corner flow of Law.[14] Good quantitative agreement with the Reda and Murphy data was obtained, but only the qualitative features of the compression corner flow were well simulated. Using a more sophisticated second-order accurate numerical scheme, Baldwin[3,4] considered both the two equation differential model of Saffman and a simpler algebraic mixing-length model to simulate the hypersonic shock boundary-layer interaction experiment of Holden.[15] He found the more elaborate model of Saffman to yield somewhat better results than the algebraic model, but at the cost of considerably more computing time. Good quantitative agreement with experiment was not obtained with either model. Following Baldwin's approach all subsequent investigations have been performed using the more rigorous second-order accurate numerical scheme of MacCormack.[17,18] Deiwert[5,6,11] considered an algebraic mixing-length model to simulate the transonic airfoil experiment of McDevitt et al.[16] while Horstman et al.[8] used a similar approach to simulate their hypersonic shock boundary-layer experiment on an axisymmetric cylinder. In each of these studies, while qualitative features of the flows were described well, good quantitative agreement with experiment in the interaction regions was not obtained.

Using a relaxing turbulence model Shang and Hankey[7] simulated the compression corner flow of Law, and Baldwin and Rose[10] simulated the flat plate flow of Reda and Murphy. In each of these studies the relaxing model was found to perform significantly better than the simpler algebraic model and, according to Shang and Hankey, provided significantly better comparisons with measurements than were obtained by Wilcox using the two equation differential model of Saffman.

In each of these studies it was essential that the full Navier-Stokes equations be considered to describe the viscous-inviscid interaction and the elliptic nature of separating-reattaching flows properly. Because of the large computing times necessary to solve these equations, turbulence closure by the simplest model forms is an important practical consideration. For example, Baldwin found that using the Saffman two equation differential model required an order of magnitude more computing time for the hypersonic shock boundary-layer interaction computation than did the simpler algebraic eddy viscosity mode. For the more slowly converging transonic computations[5,6] this increase in computer time would be prohibitive. The question of concern is then: Are the algebraic eddy viscosity models capable of adequately supporting a numerical description of this complex turbulent flow?

The recent efforts by Shang and Hankey and by Baldwin and Rose indicate that for the supersonic flat plate and compression corner flows, a relaxing algebraic model may be adequate. For the more general transonic flowfield over airfoil configurations, the answer is less clear. Essential features of the transonic airfoil flow not exhibited in either the flat plate or compression corner flows include: 1) a nonequilibrium turbulent boundary-layer flow ahead of the interaction region, 2) a free interaction between the inviscid shock and the turbulent boundary layer, 3) the possibility of two distinct separation regions (both shock induced and trailing edge induced) or one large merged region, 4) the existence of exceptionally thick separation bubbles, and 5) a free reattachment in a turbulent wake. Clearly, flows of this type provide a stringent test for any turbulent transport model.

Described here are the results of a series of computations using various algebraic eddy viscoisity model formulations to simulate the transonic turbulent flowfield over an 18% thick symmetric circular-arc airfoil. The results are compared with recent wind-tunnel experiments[16] in an attempt to assess the validity of the models and to provide some insight for future model formulations.

## Procedure

The flow under consideration (illustrated in Fig. 1) is the transonic turbulent flow over a symmetric 18% thick circular

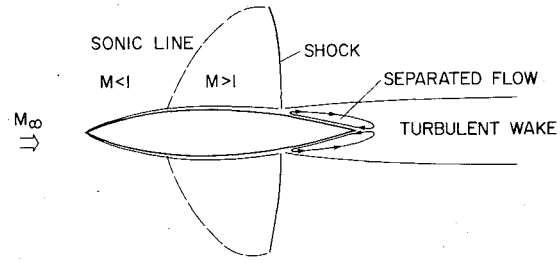


**Fig. 1 Transonic flow over 18% circular-arc airfoil, shown schematically.**

Presented as Paper 75-829 at the AIAA 8th Fluid and Plasma Dynamics Conference, Hartford, Conn., June 16-18, 1975; submitted June 26, 1975; revision received November 21, 1975.

Index category: Aircraft Aerodynamics (including Component Aerodynamics).

*Research Scientist, Computational Fluid Dynamics Branch. Member AIAA.

arc airfoil at zero angle of attack. At sufficiently high subsonic freestream Mach numbers the flow accelerates over the forward portion of the airfoil and enters a supersonic region. This supersonic flow region terminates over the aft portion of the airfoil by means of a standing shock. This shock wave is free to interact with the existing boundary layer on the airfoil surface, which is likely to be turbulent at the high Reynolds numbers associated with transonic speeds. For large enough pressure jumps across the shock the boundary layer will separate. In any event, for the thick airfoil under consideration, the flow will always be separated near the trailing edge. It is possible for these two separation regions to coalesce and form one large separation bubble. This can significantly alter the inviscid flowfield over an airfoil, thus changing its lift and drag characteristics.

Experimental results[16] indicate that, for the 18% circular arc, the flow is steady with trailing edge separation for freestream Mach numbers below 0.755 and steady with coalesced shock induced-trailing edge separation for freestream Mach numbers greater than 0.782. For freestream Mach numbers between 0.755 and 0.782, the flow may be periodically unsteady, alternating between the two separation modes.

The equations appropriate to describe the steady flow are the two-dimensional compressible Navier-Stokes equations. These equations, written in time-dependent Reynolds averaged form, can be solved by the explicit finite-difference method of MacCormack as described in Refs. 5, 6, and 9. Repeated here for completeness the equations are

$$\frac{\partial}{\partial t}\int_{\text{vol}} U \,\mathrm{d}\,\text{vol} + \int_S \vec{H}\cdot\,\vec{n}\,\mathrm{d}s = 0$$

where

$$U \equiv \begin{Bmatrix} \rho \\ \rho u \\ \rho v \\ e \end{Bmatrix} \qquad \vec{H} \equiv \begin{Bmatrix} \rho\vec{q} \\ \rho u\vec{q} + \vec{\tau}\cdot\,\vec{e}_x \\ \rho v\vec{q} + \vec{\tau}\cdot\,\vec{e}_y \\ e\vec{q} + \vec{\tau}\cdot\,\vec{q} - k\nabla T \end{Bmatrix}$$

$$\vec{q} \equiv u\vec{e}_x + v\vec{e}_y$$

$$\vec{\tau} \equiv \sigma_x e_x \vec{e}_x + \tau_{xy}\vec{e}_x\vec{e}_y + \tau_{yx}\vec{e}_y\vec{e}_x + \sigma_y\vec{e}_y\vec{e}_y$$

and $\vec{e}_x$, $\vec{e}_y$ are unit vectors in orthogonal $x$, $y$ space and $\vec{n}$ is a unit normal vector to the surface element $ds$ about the volume element vol.

The turbulence modeling is incorporated in the shear stress terms $\tau_{xy}$ and $\tau_{yx}$ in the form of an eddy viscosity coefficient $\epsilon$ as

$$\tau = \tau_{xy} = \tau_{yx} = (\mu + \rho\epsilon)\,[(\partial u/\partial y) + \partial v/\partial x)]$$

All of the models considered in the present study are algebraic "two layer" descriptions with separate formulations for the inner and outer regions of the attached boundary layer and separate formulations for the separation bubble and for the airfoil wake. All the computations in the present study were performed using a $50 \times 38$ mesh corresponding to the flow and transverse directions, respectively. The control volume was 16 chords long and 6 chords high and the mesh stretched exponentially away from the airfoil in each direction. Twenty mesh points were distributed uniformly over the airfoil surface, ten ahead of the airfoil, and twenty downstream of the trailing edge. The transverse mesh consisted of three exponentially stretched layers corresponding to the sublayer (four points), boundary layer (nine points), and the outer inviscid flow. Computations were performed with both a primitive Illiac IV code and a sophisticated CDC 7600 code, each with run times of typically 1 hr to reach steady state (assumed achieved in a dimensionless time, $tU_\infty/c$, of 8).

## Results

### Model 1

The first model considered, model 1, uses a van Driest[19] damping formulation in the inner region and a plane mixing formulation in the outer region. No special consideration is given to the separated regions, and the airfoil wake is described by a plane mixing layer of the Clauser[20] type. Used in the previous studies[5,6,9,11] the model is repeated here:

Inner region

$$\epsilon = \ell^2\,|(\partial u/\partial y) + (\partial v/\partial x)| \tag{1}$$

$$\ell = 0.40\,y[1-\exp(-y/A)] \tag{2}$$

Outer region

$$A = 26\frac{\mu_w}{\rho_w}(\rho_w/\tau_w)^{1/2} \tag{3}$$

$$\ell = 0.07\,(\delta - y_0) \tag{4}$$

where $\delta$ is the boundary layer thickness and $y_0$ is the farthest point across the boundary layer where the velocity is zero. (for attached boundary layers $y_0 = 0$). The eddy viscosity is then given by Eq. (1).

Airfoil wake

$$\epsilon = 0.001176(\delta - y_0)\,|u_\delta - u_{\text{℄}}| \tag{5}$$

where $u_{\text{℄}}$ is the velocity at the edge of the wake and $u_{\text{℄}}$ is the velocity at the centerline. The molecular and turbulent Prandtl numbers are assumed equal at a value of 0.90.

While certain trends may be predicted by using eddy-viscosity model 1 as indicated in Ref. 5 the details in the interaction region are not properly described. A close look at the eddy-viscosity model reveals that two parameters are rather poorly defined in the interaction region. First, the effective "diffusion velocity" given by $\ell|\partial u/\partial y + \partial v/\partial x|$ in the inner region undergoes unrealistic excursions near zero in the reverse-flow region. This is due, in part, to the velocity gradient $|\partial u/\partial y + \partial v/\partial x|$ approaching zero and, in part, to the van Driest damping term $[1-\exp(-y/A)]$ approaching zero as $\tau_w$ becomes small. Second, the determination of the length scale $\delta$ in the outer region is somewhat arbitrary in the interaction region, where gradients caused by the shock extend far into the inviscid part of the flowfield.

### Model 2

To counter both of the aforementioned difficulties a second model, model 2, is considered as follows:

Inner region

$$\epsilon = \ell^2\left[\left(\frac{\partial u}{\partial y}\right)^2 + \left(\frac{\partial v}{\partial x}\right)^2\right]^{1/2} \tag{6}$$

$$\ell = 0.41\,y[1-\exp(-y/A)] \tag{7}$$

Outer region

$$\epsilon = 0.0168\,u_\delta\delta_i^*/\left[1 + \left(\frac{y-y_0}{\delta}\right)^6\right] \tag{8}$$

$$\delta_i^* = \int_{y_0}^{\delta}(1-u/u_\delta)\,\mathrm{d}y \tag{9}$$

Separation bubble

$$\epsilon = \ell^2 \max\left\{\left[\left(\frac{\partial u}{\partial y}\right)^2 + \left(\frac{\partial v}{\partial x}\right)\right]^{1/2}, \frac{u_\delta}{\delta}\right\} \qquad (10)$$

The airfoil wake is described by Eq. (8) and the molecular and turbulent Prandtl numbers are 0.72 and 0.90, respectively.

This second formulation, with the effective "diffusion velocity" used in Eqs. (6) and (10), is less likely to approach zero, due to local velocity gradients, than model 1. Furthermore, in the separation bubble itself the velocity gradient term is replaced by the mean gradient $u_\delta/\delta$ when it becomes small. Clauser's formulation is used in the outer region where the less ambiguous length scale, the kinematic displacement thickness $\delta_i^*$, has replaced the boundary-layer thickness $\delta$ used in model 1. The length $\delta$ is still used in Eq. (8) in the intermittency factor $[(y-y_0)/\delta]^6$, in Eq. (9) as the upper limit on the displacement integral, and in the mean velocity gradient in the separation bubble [Eq. (10)], but these are all less sensitive areas than the outer length scale usage in model 1. The determination of the length scale $\delta_i^*$ in the separation region, however, is somewhat arbitrary and may be critical in flows with large separation bubbles. In Eq. (9) the integration is performed from $y_0$ to the boundary layer edge $\delta$, where $y_0$ is the farthest point across the boundary layer where the velocity is zero. This selection of $y_0$ instead of $y=0$ is necessary to avoid unrealistic length scales in the reverse-flow regions. Displacement effects in regions of massive separation can be orders of magnitude larger than in attached-flow regions, resulting in very large length scales if the integration is performed through the reverse-flow region.

Comparisons of computed surface pressure distributions using models 1 and 2 are shown in Fig. 2 for a freestream Mach number of 0.775 and a chord Reynolds number of two million. Included in this figure are the computed inviscid pressure distribution and experimental results obtained by McDevitt et al. For all three computations the agreement with experiment ahead of the interaction region is excellent. In the interaction region itself the viscous solutions predict the experimental results much better than the inviscid solution, with the results using model 2 showing a marked improvement over model 1. Over the trailing edge both viscous solutions indicate more extensive separation effects than does the experiment. This is denoted by the computed pressure plateau over the separation bubble over the last 20% of chord. This disparity may be due, in part, to possible unsteadiness in the experiment which, according to Ref. 16, is likely to exist over the last 25% of chord. In any event, the improvement of viscosity model 2 over model 1 is sufficient to neglect model 1 from further consideration.

To avoid comparisons with experimentally unsteady flow, viscosity model 2 was used to compute both a weak interaction flow ($M_\infty = 0.7425$) and a strong interaction flow ($M_\infty = 0.788$) where experiments are known to be steady. Results for these flowfields are shown in Fig. 3 for a chord Reynolds number of four million. The shadowgraphs at the top of Fig. 3 are of the aft region of the experimental flowfield corresponding to the low and high Mach numbers. The shadowgraph at the left, for the lower Mach number, shows a nearly normal shock at about 63% of chord. The boundary layer behind the shock remains attached yet shows substantial thickening. Near the trailing edge, it separates, denoted by the sudden change in curvature of the boundary-layer edge and the massive thickening of the viscous region itself. The shadowgraph at the right shows an oblique shock at about 65% of chord. The flow behind the shock is separated, as evidenced by the flow pattern behind the shock, and reattached downstream in the wake. The separation bubble is quite thick, as evidenced both by the existence of the oblique shock necessary to turn the flow and by the thickness of the viscous region itself.

Computed Mach contours for the same flow conditions are shown immediately beneath the shadowgraphs. Lines of constant Mach number are shown in increments of 0.02. For the lower Mach number case, on the left the shock is centered about the 73% chord, in agreement with the computed surface pressure distribution. The boundary layer behind the shock thickens but remains attached until near the trailing edge, where it separates. The flowfield details indicated in both the shadowgraph and contour plot are remarkably similar in character, although they differ in quantitative detail. For the higher Mach number flow on the right the shock is normal away from the airfoil surface and becomes oblique in the interaction region. The shock is centered near the 70% chord near the surface. The flowfield behind the shock is separated and reattached in the wake. Except for some differences in shock position and orientation the computed flowfield is remarkably similar to that given by experiment in a qualitative sense.

Finally, at the bottom of Fig. 3 computed velocity vector plots near the airfoil surface indicate the magnitude and direction of the flow. For the lower Mach number the separation region is small and confined to the vicinity of the trailing edge. For the higher Mach number the separation region extends from the shock impingement area into the wake and is noticeably thick.

**Models 3 and 4**

It is obvious from the results computed using algebraic models 1 and 2 in the present study that it is possible to

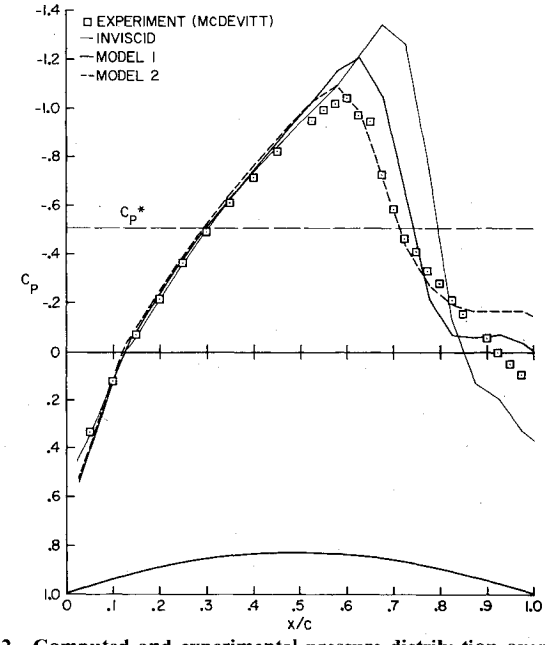


**Fig. 2 Computed and experimental pressure distribution over 18% circular arc; $M_\infty = 0.775$; $Re_c = 2 \times 10^6$.**

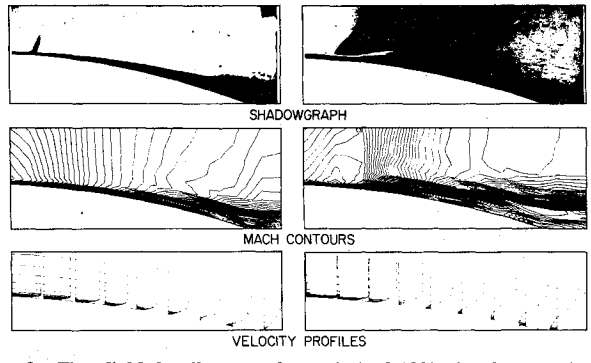


**Fig. 3 Flowfield details over aft portion of 18% circular-arc airfoil; experiment: McDevitt,[16] computation: model 2. $Re_c = 4 \times 10^6$; $t/c = 0.18$; $M_\infty = 0.7425$ (left); $M_\infty = 0.788$ (right).**

simulate the basic features of the separating transonic turbulent flowfields. It is equally obvious that these simple models did not permit quantitative prediction of experimental results in the interaction and separation regions. Following the suggestions of several investigators McDonald and Stoddart[21,22] and Goldberg[23] independently formulated and applied differential relaxation procedures to account for the effect of flow history on turbulent shear in regions of adverse pressure gradients. Rotta[24] has indicated that the life of the large eddies is equivalent to a distance one order of magnitude greater than the boundary-layer thickness. Nash and Hicks[25] used this length scale and applied McDonald and Stoddart's approach for incompressible turbulent boundary layers. Deiwert and Abbott[26] applied Goldberg's expression based on momentum thickness with similar effectiveness. Reyhner[27] used a similar lag equation for eddy viscosity in conjunction with a differential boundary-layer program. More recently, Bradshaw[28] on the basis of experimental studies by Deissler[29] and by Narasimha and Prabhu,[30] and Rose and Johnson,[31] on the basis of their own experiments proposed similar differential relaxation procedures for the turbulent length scales. Baldwin and Rose used this concept to simulate the flat plate interaction flow of Reda and Murphy and found significant improvement over local algebraic models. Shang and Hankey simulated the compression corner flow of Law in a similar manner and found even better performance than the more elaborate two equation differential mode of Saffman, as used by Wilcox for computing the same flowfield. With this background of success it seemed reasonable to try a similar approach in the present study.

As a first attempt in using the relaxation concept the following baseline model, model 3, is defined with the different regions indicated in Fig. 4.

I. Inner region – Eqs. (6) and (7)

II. Outer region and wake

$$\epsilon = 0.0168\, u_\delta \delta_i^* / \left[1 + \left(\frac{y - y_{DS}}{\delta}\right)^6\right] \tag{11}$$

$$\delta_i^* = \int_{y_{DS}}^{\delta} (1 - u/u_\delta)\, dy \tag{12}$$

and $y_{DS}$ is the location of the dividing streamline

III. Separation bubble wall region

$$\epsilon = 0.0168\, u_\delta \delta_i^* \{ (y/y_{DS}) [1 - \exp(-y/A)] \}^2 \tag{13}$$

IV. Separation bubble wake region

$$\epsilon = 0.0168\, u_\delta \delta_i^* \tag{14}$$

The molecular and turbulent Prandtl numbers are 0.72 and 0.90, respectively.

There are two essential differences between model 3 and model 2. First, the kinematic displacement thickness $\delta_i^*$ is measured from the dividing streamline in model 3 rather than from the zero velocity line. Second, the eddy viscosity distribution inside the separation bubble is determined by interpolating between the dividing streamline and the airfoil surface or wake centerline in model 3 rather than being based on local flow properties, as in models 1 and 2. The ad hoc interpolation function in the wall region is quadratic in terms of the distance $y$ and the van Driest damping function; in the wake region it is constant. In this manner the separation bubble is separated from the rest of the viscous flowfield by the dividing streamline, and the eddy viscosity distribution across the bubble may be more reasonably controlled than with the arbitrarily imposed boundary-layer formulation used in models 1 and 2.

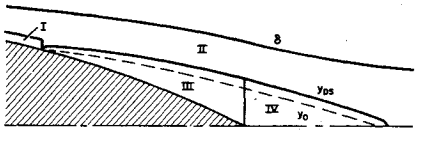


Fig. 4 Model 3 viscosity regions.

Referring to the above model 3 as the "equilibrium" value $\epsilon_{eq}$, the following relaxation model (model 4) can be used to account for history and pressure gradient effects:

$$\epsilon(\xi) = \epsilon(\xi - \Delta\xi) + [\epsilon_{eq}(\xi) - \epsilon(\xi - \Delta\xi)]\, [1 - \exp(-\Delta\xi/\lambda)] \tag{15}$$

where $\xi$ is the streamwise location where $\epsilon$ is evaluated and $(\xi - \Delta\xi)$ is upstream a distance $\Delta\xi$ along a streamline. In actual practice $\Delta\xi$ in the exponential is approximated by $\Delta x$, which, in all present computations, was one mesh spacing, but $\epsilon(\xi)$, $\epsilon(\xi - \Delta\xi)$, and $\epsilon_{eq}(\xi)$ are all evaluated on the same streamline.

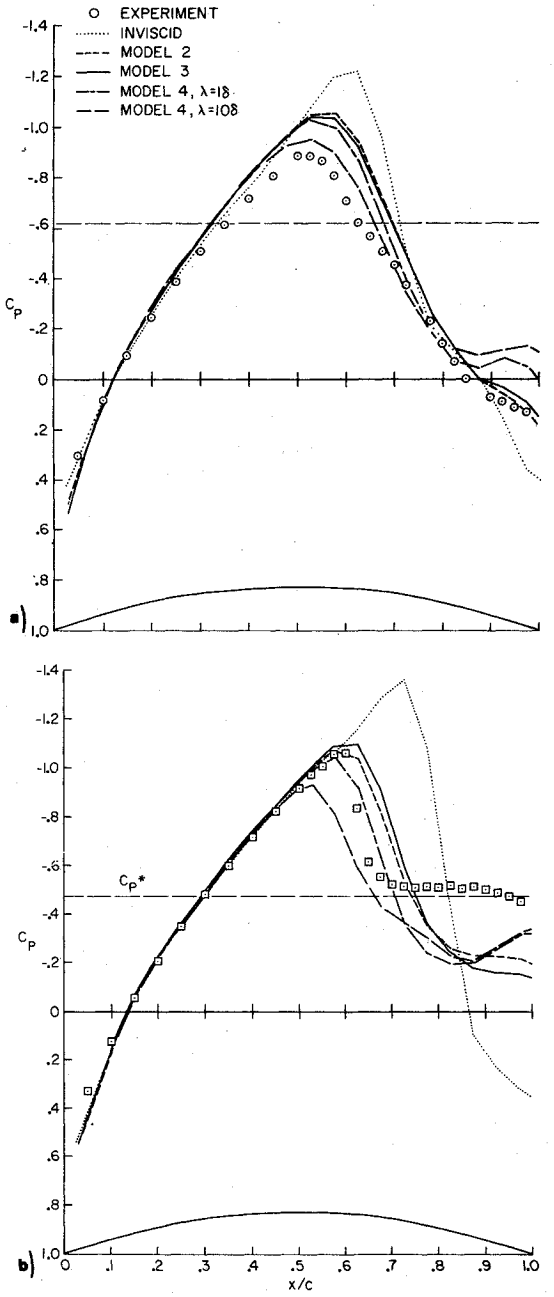


Fig. 5 Effect of relaxation on surface pressure distribution over 18% circular arc; $Re_c = 4 \times 10^6$; a) $M_\infty = 07425$; b) $M_\infty = 0.788$.

Because the memory in the inner region is short and because the separation bubble is isolated by the dividing streamline, the relaxation equation [Eq. (15)], is applied only to the outer region and wake (region II in Fig. 4). The discontinuity between regions I and II at the separation point is somewhat alleviated by relaxing along the streamlines from region I into region II. This should contribute to better performance as compared with the unrelaxed model 3.

The symbol $\lambda$, which is a relaxation parameter, may be a function of the solution. When $\lambda = 0$ there is no relaxation and the model reverts back to the baseline model 3. For large $\lambda$ the relaxation is strong and upstream history will have a large influence. Three different values of this parameter have been considered in the present study: $\lambda = 0$ (baseline model 3), $\lambda = \delta$ (moderate relaxation), and $\lambda = 10\delta$ (strong relaxation). In the second and third cases $\lambda$ is a function of the solution in terms of the boundary-layer thickness $\delta$. The value of $10\delta$ has been suggested by Rotta, Bradshaw, Rose and Johnson, and others, and was used by Shang and Hankey and Baldwin and Rose in their studies. In both of these studies, however, the relaxation was carried out not along streamlines but along lines parallel to the solid surface. The present computations are believed to be the first whereby the relaxation is actually along the streamlines.

Surface pressure distributions computed with models 2, 3, and 4 are compared in Fig. 5 with experiment and inviscid computations for flows at Mach numbers of 0.7425 and 0.788 and a chord Reynolds number of 4 million. In Fig. 5a for $M_\infty = 0.7425$ the differences between the baseline model 3 results and the model 2 results are slight. As the relaxation parameter $\lambda$ is increased to $1\delta$, then to $10\delta$, the computed pressure distributions over the forward 80% of the airfoil approach the experiment more closely. At the trailing edge, however, separation effects increase and the computed results deviate more from the experiment. A possible explanation for this may be that values of eddy viscosity in region II over the separation bubble are too small because of too short a length scale. This would encourage the bubble to grow larger than if the viscosity outside the bubble were greater. It will be recalled that the definition of $\delta_I^*$ in this region was somewhat arbitrary. The experimental data over the midchord region may be somewhat low at this lower Mach number, due to off-design wind-tunnel wall contouring. The wind-tunnel walls were contoured to match the computed streamlines for $M_\infty = 0.775$.

In Fig. 5b for $M_\infty = 0.788$ the differences between the results for baseline model 3 and model 2 are again slight, with the model 2 solution looking slightly better. As the relaxation parameter is increased to $1\delta$, the computed pressure distribution over the forward 70% of the airfoil approaches the experiment more closely. As the relaxation parameter is further increased to $10\delta$, the computed pressure distribution is overcorrected. The pressure jump across the shock is still greater than that demonstrated by experiment, although it tends to readjust over the separation region itself. This suggests a shock that does not have enough obliqueness. This would imply a smaller turning angle of the flow over the separation point, indicating a separation bubble that does not grow rapidly enough in the interaction region. This is probably due to incorrect behavior of the turbulence model in the vicinity of separation, so that the growth rate of the separation bubble is computed incorrectly.

Figure 6 shows typical computed eddy viscosity distributions for model 4 for $M_\infty = 0.788$ both ahead of and through the separation region at chord locations of 62.5%, 72.5%, 92.5%, and in the wake at 107.9%. In all instances the unrelaxed distributions have the largest magnitude and the highly relaxed distributions ($\lambda = 10$) have the lowest magnitude of eddy viscosity. At $x/c = 0.725$, just after separation, the unrelaxed eddy viscosity distribution shows unrealistically large values near the wall. This is due to the discontinuity in the turbulence model at the separation point, which is somewhat alleviated by relaxation. For the unrelaxed model and for small relaxation ($\lambda = 1\delta$) the eddy viscosity over the separation bubble is larger than it was ahead of the interaction. For the large relaxation ($\lambda = 10\delta$) the reverse is true.

Smaller values of eddy viscosity lead to larger separation bubbles. This is illustrated in Fig. 7, which shows the dividing streamlines computed using model 4 for $M_\infty = 0.788$ and a chord Reynolds number of 4 million. As the relaxation parameter is increased from $\lambda = 0$ to $1\delta$, which is accompanied by a corresponding decrease in the magnitude of eddy viscosity, the separation bubble is seen to grow in all directions. Unfortunately, there is not yet sufficient experimental evidence to describe the extent of the separation region. However, laser velocimeter experiments are in progress in the Ames High-Reynolds-Number Channel which will provide these data and should be helpful in devising and further testing of turbulence models.

## Conclusions

The transonic turbulent flowfield over a symmetric 18% thick circular arc airfoil has been numerically simulated by solving the two-dimensional time-dependent Reynolds averaged compressible Navier-Stokes equations. Turbulence closure was achieved by a variety of algebraic eddy viscosity models, with special consideration given to regions of shock boundary-layer interaction and flow separation. Computed solutions were compared with recent experiemental results obtained in the Ames High-Reynolds-Number Channel. Each of the eddy viscosity models was found capable of supporting a qualitative description of the flowfield. Quantitative details in the interaction and separation region, however, were not good. The probable reason for this is inadequate modeling in the vicinity of the separation point and through the entire separated region. Additional flexibility can be achieved by using relaxation to account for history and pressure gradient effects. While this leads to improved agreement with experimental results, the essential problem of modeling the shear in the separated region remains. The limited success

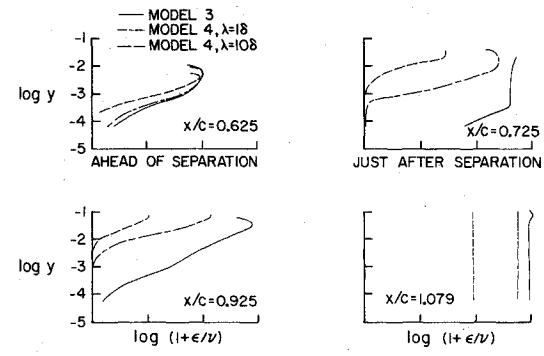


**Fig. 6 Typical computed eddy viscosity distributions in the vicinity of separation; $M_\infty = 0.788$; $Re_c = 4 \times 10^6$.**

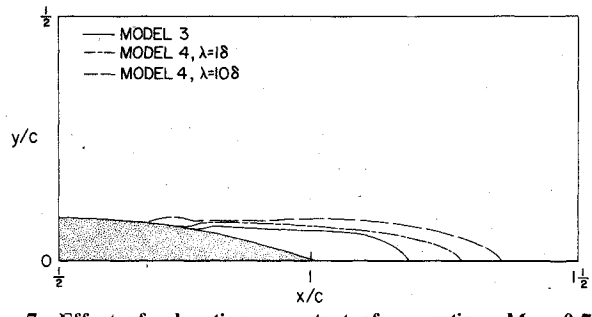


**Fig. 7 Effect of relaxation on extent of separation; $M_\infty = 0.788$; $Re_c = 4 \times 10^6$.**

achieved in this study encourages the view that algebraic eddy viscosity models incorporating relaxation effects may be found that will provide reasonable descriptions of separated flowfield of the type under investigation. With the advent of more detailed experimental measurements in the interaction and separation regions, the development of more appropriate eddy viscosity models seems likely.

## References


[1]Wilcox, D.C., "Calculation of Turbulent Boundary-Layer Shock Wave Interaction," *AIAA Journal,* Vol. 11, April 1973, pp. 1592-1594.

[2]Wilcox, D. C., "Numerical Study of Separated Turbulent Flows," AIAA Paper 74-584, Palo Alto, Calif., 1974.

[3]Baldwin, B. S. and MacCormack, R. W., "Numerical Solution of the Interaction of a Strong Shock Wave with a Hypersonic Turbulent Boundary Layer," AIAA Paper 74-588, Palo Alto, Calif., 1974.

[4]Baldwin, B. S. and MacCormack, R. W., "Interaction of Strong Shock Wave with Turbulent Boundary Layer," *Lecture Notes in Physics,* Vol. 35, Springer-Verlag, Berlin, Germany, 1975, p. 51-57.

[5]Deiwert, G. S., "Numerical Simulation of High Reynolds Number Transonic Flows," *AIAA Journal,* Vol. 13, Oct. 1975, pp. 1354-1359.

[6]Deiwert, G. S., "High Reynolds Number Transonic Flow Simulation," *Lecture Notes in Physics,* Vol. 35, Springer-Verlag, Berlin Germany, 1975, p. 132.

[7]Shang, J. S. and Hankey, W. L., Jr., "Numerical Solution of the Navier-Stokes Equations for Supersonic Turbulent Flow over a Compression Corner," AIAA Paper 75-34, Pasadena, Calif., 1975.

[8]Horstman, C. C., Kussoy, M. I., Coakley, T. J., Rubesin, M. M., and Marvin, J. G., "Shock-Wave-Induced Turbulent Boundary-Layer Separation at Hypersonic Speeds," AIAA Paper 75-433, Pasadena, Calif., 1975.

[9]Baldwin, B. S., MacCormack, R. W., and Deiwert, G. S., "Numerical Techniques for the Solution of the Compressible Navier-Stokes Equations and Implementation of Turbulence Models," AGARD-LSP-73, 1975.

[10]Baldwin, B. S. and Rose, W. C., "Calculation of Shock-Separated Turbulent Boundary Layers," *Proceedings NASA Conference on Aerodynamic Analyses Requiring Advanced Computers,* Langley, Va., NASA SP-347, March 1975, pp. 361-373.

[11]Deiwert, G. S., McDevitt, J. B., and Levy, L. L. Jr., "Simulation of Turbulent Transonic Separated Flow," *Proceedings NASA Conference on Aerodynamic Analyses Requiring Advanced Computers,* Langley, Va., NASA SP-347, March 1975, pp. 419-436.

[12]Saffman, P. G., "A Model for Inhomogeneous Turbulent Flow," *Proceedings of the Royal Society of London,* Vol. A317, 1970, pp. 417-423.

[13]Reda, D. C. and Murphy, J. D., "Shock Wave-Turbulent Boundary Layer Interactions in Rectangular Channels," AIAA Paper 72-234, 1972.

[14]Law, C. H., "Supersonic Turbulent Boundary-Layer Separation Measurements at Reynolds Numbers of $10^7$ to $10^8$," *AIAA Journal,* Vol. 12, June 1974, pp. 794-797.

[15]Holden, M. S., "Shock Wave-Turbulent Boundary Layer Interaction in Hypersonic Flow," AIAA Paper 72-74, San Diego, Calif., 1975.

[16]McDevitt, J. B., Levy, L. L. Jr., and Deiwert, G. S., "Transonic Flow about a Thick Circular-Arc Airfoil," AIAA Paper 75-878, Hartford, Conn., 1975.

[17]MacCormack, R. W., "Numerical Solution of the Interaction of a Shock Wave with a Laminar Boundary Layer," *Lecture Notes in Physics,* Vol. 8, Springer-Verlag, Berlin, Germany, 1971, pp. 151-163.

[18]MacCormack, R. W. and Paullay, A. J., "Computational Efficiency Achieved by Time Splitting of Finite Difference Operators," AIAA Paper 72-154, 1972.

[19]van Driest, E. R., "On Turbulent Flow Near a Wall," *Journal of Aeronautical Sciences,* Vol. 23, Nov. 1956, p. 1007-1011.

[20]Clauser, F. H., "The Turbulent Boundary Layer," *Advances in Applied Mechanics,* Vol. IV, Pt. 1, Academic Press, New York 1956, pp. 1-51.

[21]McDonald, H. and Stoddart, J. A. P., "On the Development of the Incompressible Boundary Layer," British Aircraft Corp., Preston, England, Aero Rept. AC 223, 1965.

[22]McDonald, H. and Stoddart, J. A. P., "On the Development of the Incompressible Turbulent Boundary Layer," *Aeronautical Research Council R&M* 3484, 1967.

[23]Goldberg, P., "Upstream History and Apparent Stress in Turbulent Boundary Layers," MIT Gas Turbine Lab. Rept. 85, 1966.

[24]Rotta, J. C., "Turbulent Boundary Layers in Incompressible Flow," *Progress in Aeronautical Sciences,* Vol. 3, 1962, pp. 1-220.

[25]Nash, J. F. and Hicks, J. G., "An Integral Method Including the Effect of Upstream History on the Turbulent Shear Stress," *Proceedings of 1968 AFOSR-IFP-Stanford Conference on Computation of Turbulent Boundary Layers,* Stanford Univ., Stanford, Calif., Vol. 1, 1968, pp. 37-45.

[26]Deiwert, G. S. and Abbott, D. E., "Application of the Method of Weighted Residuals to the Turbulent Boundary-Layer Equations," *Proceedings of 1968 AFOSR-IFP-Stanford Conference on Computation of Turbulent Boundary Layers,* Stanford Univ., Stanford, Calif., Vol. 1, 1968, pp. 46-53.

[27]Reyhner, T., "Finite Difference Solution of the Compressible Turbulent Boundary-Layer Equations," *Proceedings of 1968 AFOSR-IFP-Stanford Conference on Computation of Turbulent Boundary Layers,* Stanford Univ., Stanford, Calf., Vol. 1, 1968, pp. 375-383.

[28]Bradshaw, P., "Effects of Streamline Curvature on Turbulent Flow," AGARDograph 169, (AGARD-AG-169), 1973.

[29]Deissler, R. G., "Evolution of a Moderately Short Turbulent Boundary Layer in a Severe Pressure Gradient," *Journal of Fluid Mechanics,* Vol. 64, Pt. 4, July 1974, p. 763-774.

[30]Narasimha, R. and Prabhu, A., "Equilibrium and Relaxation in Turbulent Wakes," *Journal of Fluid Mechanics,* Vol. 54, Pt. 1, July 1972, pp. 1-17.

[31]Rose, W. E. and Johnson, D. A., "Turbulence in a Shock-Wave Boundary-Layer Interaction," *AIAA Journal,* Vol. 13, July 1975, pp. 884-889.